Leveraged ETF options implied volatility paradox: a statistical study [*]

Wolfgang Karl Härdle, [†]   Sergey Nasekin, [‡]   Zhiwu Hong [§]

November 13, 2016

[†]C.A.S.E.- Center for Applied Statistics & Economics, Humboldt-Universität zu Berlin, Spandauer Str. 1, 10178 Berlin, Germany; Singapore Management University, 50 Stamford Road, 178899 Singapore, Singapore (*e-mail: haerdle@hu-berlin.de; telephone: +49 30 2093-5631*)

[‡]C.A.S.E.- Center for Applied Statistics & Economics, Humboldt-Universität zu Berlin (*e-mail: nasekins@hu-berlin.de; telephone: +49 30 2093-1470*) (corresponding author)

[§]Wang Yanan Institute for Studies in Economics (WISE), Xiamen University (*e-mail: hzw1888@126.com*)

Abstract

In this paper, we study the statistical properties of the moneyness scaling transformation by Leung and Sircar (2015). This transformation adjusts the moneyness coordinate of the implied volatility smile in an attempt to remove the discrepancy between the IV smiles for levered and unlevered ETF options. We construct bootstrap uniform confidence bands which indicate that there remains a possibility that the implied volatility smiles are still not the same, even after moneyness scaling has been performed. This presents possible arbitrage opportunities on the (L)ETF market which can be exploited by traders. An empirical data application shows that there are indeed such opportunities in the market which result in risk-free gains for the investor. A dynamic "trade-with-the-smile" strategy based on a dynamic semiparametric factor model is presented. This strategy utilizes the dynamic structure of implied volatility surface allowing out-of-sample forecasting and information on unleveraged ETF options to construct theoretical one-step-ahead implied volatility surfaces. Additionally, we propose a semi-analytic and a simulation-based estimation approach for incorporating stochastic volatility into the moneyness scaling method. This approach allows to infer the "expected integrated variance smile" from the data.

Key words: exchange-traded funds, options, moneyness scaling, arbitrage, bootstrap, dynamic factor models

JEL Classification: C00, C14, C50, C58

Introduction

Exchange-traded funds (ETFs) are financial products that track indices, commodities, bonds, baskets of assets. They have become increasingly popular due to diversification benefits as well as the investor's ability to perform short-selling, buying on margin and lower expense ratios than, for instance those of mutual funds.

The trading advantages of the ETFs are enhanced through the use of gearing or leverage, when derivative products are used to generate multiple or inverse multiple returns on the underlying asset. For instance, the leveraged ETF ProShares Ultra

S&P500 (SSO) with leverage ratio $\beta = +2$ is supposed to gain 2% for every 1% daily gain in the price of the S&P500 index, with a subtraction of an expense fee. An inverse leveraged ETF would invert the loss and amplify it proportionally to the ratio magnitude: the ProShares UltraShort S&P500 (SDS) with leverage ratio $\beta = -2$ would generate a 2% gain for every 1% daily loss in the price of the underlying S&P500 index. Naturally, the basic unleveraged SPDR S&P 500 ETF (SPY) returns 100% of the gain/loss of S&P 500 index, having $\beta = +1$.

Due to their growing popularity and the nature of ETF and LETF similar dynamics, recently there has been growing research on leveraged ETFs and their consistent pricing. Specifically, Leung and Sircar (2015) introduced the so-called "moneyness scaling" technique which links implied volatilities (IV) between ETF and LETF in the way that the discrepancy between the implied volatility "smile" pattern is removed. Recent empirical observations seemingly support this idea. Figure 1 below compares the empirical implied volatilities for the LETFs SSO, SDS, UPRO ($\beta = +3$), SPXU ($\beta = -3$) before moneyness scaling is done. The log-moneyness LM is defined as

$$LM \stackrel{\text{def}}{=} \log\left(\frac{K}{L_t}\right), \tag{1}$$

where K is the strike of the LETF option and L_t the LETF price at time t. After implied volatility re-scaling according to the identity

$$\sigma_{LETF}^{resc.} \stackrel{\text{def}}{=} |\beta|^{-1} P_{BS}^{-1}(P_\beta), \tag{2}$$

where P_{BS} is the option Black-Scholes price and P_β is an observed market price of the LETF, there are still visible discrepancies between the implied volatilities for the SPY ETF and its leveraged counterparts. The moneyness scaling procedure yields a more

coherent picture as in Figure 2, when the LETF and ETF implied volatilities overlap significantly better.

The question arises whether the moneyness scaling method indeed removes discrepancies consistently in time. To answer this question, a study is required to verify whether IV deviations are significant from the statistical point of view. This leads to the problem of constructing confidence intervals (or confidence bands) for the difference of IV estimators. Several studies including Cont and da Fonseca (2002), Aït-Sahalia et al. (2001) apply non- and semiparametric approaches to model implied volatilities. The use of such estimators allows to construct uniform or bootstrap confidence bands which can be used as a check for the potential existence of price discrepancies among ETF options with different leverage ratios.

1 Consistency study for moneyness scaling

1.1 Implied volatility as estimator

The moneyness scaling technique proposed by Leung and Sircar (2015) offers a "coordinate transformation" for the LETF option implied volatility and potentially reflects the increase of risk in the underlying asset (ETF). Based on the assumption that the distribution of the terminal price of the β-LETF depends on the leverage ratio β, the moneyness scaling formula includes an expectation of the β-LETF log-moneyness conditional on the terminal value of the unleveraged counterpart. For the LETF log-moneyness LM^{β} (consider ETFs as LETFs with $\beta = 1$) the formula linking two LETFs

with different leverage ratios β_1, β_2 takes the (approximate) form:

$$LM^{\beta_1} = \frac{\beta_1}{\beta_2} \left[LM^{\beta_2} + \{r(\beta_2 - 1) + c_2\}\tau + \frac{\beta_2(\beta_2 - 1)}{2}\overline{\sigma}^2\tau \right] - \{r(\beta_1 - 1) + c_1\}\tau$$
$$- \frac{\beta_1(\beta_1 - 1)}{2}\overline{\sigma}^2\tau \quad (3)$$

Another popular measure for moneyness is the so-called forward moneyness which is an appropriate choice for European option data because European options can be only exercised at expiry. It is defined as follows:

$$\kappa_f \stackrel{\text{def}}{=} K/\{e^{(r-c)\tau}L_t\}, \quad (4)$$

where r is the interest rate, c stock dividend ratio. In terms of the forward moneyness, the moneyness scaling equation for two LETFs with different leverage ratios β_1, β_2 can be shown (see Appendix 5.1) to satisfy:

$$\kappa_f{}^{(\beta_1)} = \exp\left\{ -\frac{\beta_1}{2}(\beta_1 - \beta_2)\overline{\sigma}^2\tau \right\} (\kappa_f{}^{(\beta_2)})^{\frac{\beta_1}{\beta_2}}. \quad (5)$$

Many researchers, among them Fengler et al. (2007), Park et al. (2009) have studied the implied volatility as a random process in time, so that the data generating process includes some non-parametric function m:

$$Y_t = m(X_t) + \varepsilon_t, \quad t = 1, \ldots, T, \quad (6)$$

or can be driven by a latent factor process $\mathcal{Z}_t$:

$$Y_t = \mathcal{Z}_t^\top m(X_t) + \varepsilon_t, \quad t = 1, \ldots, T, \quad (7)$$

where Y_t stands for an implied volatility process, the covariates X_t can be one- or multi-dimensional. Usually X_t is assumed to contain a moneyness component such as κ_f and the time-to-maturity τ.

1.2 Confidence bands

The statistical properties of the estimators $\widehat{m}(X_t)$ and $\widehat{\mathcal{Z}}_t^\top \widehat{m}(X_t)$ for the models (6) and (7) have been outlined, respectively, in, e.g., Härdle (1990), Ruppert and Wand (1994) and Park et al. (2009). To study the consistency of the implied volatility difference between the ETF and the moneyness-scaled LETF case, one needs to consider statistical differences of the corresponding estimators. Confidence band analysis may provide a first insight into the matter. An important issue about smooth confidence bands for functions is the correct probability of covering the "true" curve. One way to address it is to use the Bonferroni correction to adjust confidence levels for each pointwise confidence interval to obtain the overall confidence. On the other hand, asymptotic confidence bands generally tend to underestimate the true coverage probability, see Hall and Horowitz (2013).

An alternative approach is to use bootstrap confidence bands while the distribution of the original data is "mimicked" via a pre-specified random mechanism achieving both uniformity and better coverage. The approach of Härdle et al. (2015) proposes a uniform bootstrap bands construction for a wide class of non-parametric M and L-estimates. It is logical to use a robust M-type smoother for the estimation of (6) in the actual case of implied volatility, as IV data often suffer from outliers. The procedure runs as follows: consider the sample $\{X_t, Y_t\}_{t=1}^T$, where Y_t denotes the IV process, X_t is taken to be one-dimensional and includes the log-moneyness covariate LM^β.

1. Compute the estimate $\widehat{m}_h(X)$ by a local linear M-smoothing procedure (see Appendix 5.2) with some kernel function and bandwidth h chosen by, e.g., cross-validation.

2. Given $\widehat{\varepsilon}_t \stackrel{\text{def}}{=} Y_t - \widehat{m}_h(X_t)$; $\widehat{m}$ obtained in Step 1, do bootstrap resampling from $\widehat{\varepsilon}_t$, that is, for each $t = 1, \dots, T$, generate a random variable $\varepsilon_t^* \sim \widehat{F}_{\varepsilon|X}(z)$ and a re-sample

$$Y_t^* = \widehat{m}_g(X_t) + \varepsilon_t^*, \quad t = 1, \dots, T \tag{8}$$

   B times (bootstrap replications) with an "oversmoothing" bandwidth $g \gg h$ such as $g = \mathcal{O}(T^{-1/9})$ to allow for a bias correction.

3. For each re-sample $\{X_t, Y_t^*\}_{t=1}^T$ compute $\widehat{m}_{h,g}^*$ using the bandwidth h and construct the random variable

$$d_b \stackrel{\text{def}}{=} \sup_{x \in B} \left[\frac{|\widehat{m}_{h,g}^*(x) - \widehat{m}_g(x)| \sqrt{\widehat{f}_X(x)} \widehat{f}_{\varepsilon|X=x_t}(\varepsilon_t^*)}{\sqrt{\widehat{\mathsf{E}}_{Y|X}\{\psi^2(\varepsilon_t^*)\}}} \right], \quad b = 1, \dots, B, \tag{9}$$

   where B is a finite compact support set of $\widehat{f}_X$ and $\psi(u) = \rho'(\cdot)$, see Appendix 5.2.

4. Calculate the $1 - \alpha$ quantile d_α^* of $d_1, \dots, d_B$.

5. Construct the bootstrap uniform confidence band centered around $\widehat{m}_h(x)$:

$$\widehat{m}_h(x) \pm \left[\frac{\sqrt{\widehat{\mathsf{E}}_{Y|X}\{\psi^2(\varepsilon_t^*)\}} d_\alpha^*}{\sqrt{\widehat{f}_X(x)} \widehat{f}_{\varepsilon|X=x_t}(\varepsilon_t^*)} \right] \tag{10}$$

We use daily data in the period 20141117-20151117 to construct bootstrap confidence bands for the M-smoother of implied volatility Y given forward moneyness X. For the LETFs SSO, UPRO, SDS X is transformed via moneyness scaling formula (5). The results are shown in Figures 3, 4 and 5 for time-to-maturity 0.5, 0.6 and 0.7 years,

respectively. A closer look at the obtained bootstrap confidence bands' relative location might imply that the moneyness scaling procedure can remove the discrepancy between the implied volatilities of leveraged ETFs and their unleveraged counterpart with possible deviations for two positively leveraged ETFs (SSO and UPRO) for smaller moneyness values. Should arbitrage opportunities arise, they are quickly traded away, given that the markets for the presented ETFs are quite liquid. However, caution should be exercised as the joint hypothesis on the difference of two estimators with a single band may still be rejected.

The illustration of the confidence bands' overlap in Figure 6 shows that the bands for the SSO LETF become wider than before and are not covered by those of the unleveraged counterpart. This implies possible discrepancies not removed by the moneyness scaling procedure. Given that the moneyness scaling approximation (5) is correct, there are arbitrage opportunities in the market of SPY and SSO which may be exploited by traders at different times to maturity.

2   Moneyness scaling under stochastic volatility

2.1   A semi-analytical approach

In the study of moneyness scaling, one needs to estimate the following conditional expectation:

$$\mathbb{E}^{\mathbb{Q}}\left(\int_0^t \sigma_s^2 \mathrm{d}s \,\Bigg|\, \log\left(\frac{L_t}{L_0}\right) = LM^{(1)}\right). \tag{11}$$

As has been seen, taking $\sigma_t = \sigma$ constant, one obtains $\sigma^2 t$. As empirical evidence shows, this is not a plausible assumption, therefore one needs to determine the measure $\mathbb{Q}$ for

the case of random volatility under a model selected as "properly" as possible. Second, one needs to estimate the quantity

$$\int_0^t \sigma_s^2 \mathrm{d}s, \tag{12}$$

which is called the integrated variance or the integrated volatility and its estimation is a subject of considerable interest in financial literature.

Stochastic volatility presents a viable alternative to the constant case. One could choose among different specifications of stochastic volatility models. A general stochastic volatility model is defined through a system of stochastic differential equations, e.g.:

$$dS_t = A(t, S_t, V_t)dt + \xi(t, S_t, V_t)dW_{S,t}, \tag{13}$$

$$dV_t = B(t, S_t, V_t)dt + \sigma(t, S_t, V_t)dW_{V,t}, \tag{14}$$

for given functions $A(\cdot)$, $B(\cdot)$, $\sigma(\cdot)$, $\xi(\cdot)$ and a two-dimensional standard Wiener process $W_t \stackrel{\text{def}}{=} (W_{S,t}, W_{V,t})^\top$ such that $S_0 = s_0$, $V_0 = v_0$, $t \geq 0$, $s_0, v_0 \in \mathbb{R}$. Some special cases are models such as Heston (1993), Hull and White (1987), Schöbel and Zhu (1999) specifications. An example of a stochastic volatility system which is built of more than 2 equations, is given in Leung and Sircar (2015). However, simpler models tend to generate semi-closed-form solutions for the distributions of the log-returns $x_t \stackrel{\text{def}}{=} \log(S_t/S_{t-1})$. For the Heston model, a solution was proposed by Dragulescu and Yakovenko (2002).

The Heston model with risk-neutral dynamics under a risk-neutral measure $\mathbb{Q}$ and zero volatility risk premium is described by a two-dimensional system of stochastic

differential equations

$$dS_t = (r - q - 0.5)S_t dt + \sqrt{V_t} S_t dW_{S,t}^{\mathsf{Q}}, \tag{15}$$

$$dV_t = \kappa(\theta - V_t)dt + \sigma dW_{V,t}^{\mathsf{Q}}, \tag{16}$$

where $r - q$ are costs of carry on S_t, θ is the long-run variance level, κ is the rate of reversion to θ, σ is the "volatility of the volatility" parameter which determines the variance of V_t; $W_{S,t}$, $W_{V,t}$ are correlated with parameter ρ.

In Figures 7, 8 the densities of daily returns of the SCO LETF (ProShares Ultra-Short Bloomberg Crude Oil) are plotted against the densities implied by the geometric Brownian motion (GBM). It can be noticed that the tails of the Heston-implied densities are exponential and heavier than those of the normal distribution with the dispersion parameter equal to the long-term variance θ.

The solution to (11) can be computed in terms of inverse Fourier transforms of characteristic functions for particular stochastic volatility models.

Proposition 2.1.1. Under the Heston model given by (15)-(16), assuming zero costs of carry, the result is as follows:

$$\mathbb{E}^{\mathsf{Q}}\left(\int_0^T \sigma_s^2 ds \,\middle|\, \log\left(\frac{S_T}{S_0}\right) = LM^{(1)}\right) = \left[\int_0^T \frac{\int_0^\infty \Re\left\{\frac{S_0^{-i\phi}e^{-i\phi LM^{(1)}}}{i\phi}f_1(\phi)\left(\frac{\partial C_1}{\partial t} + \frac{\partial D_1}{\partial t}V_0\right) \right. }{\int_0^\infty \Re\left\{S_0^{-(i\phi+2)}e^{-LM^{(1)}(i\phi+2)} \right.} dt\right.$$
$$\left. \frac{\left. -f_2(\phi)\left(\frac{\partial C_2}{\partial t} + \frac{\partial D_2}{\partial t}V_0\right)\right\}\mathrm{d}\phi}{\left. \times f_1(\phi) + S_0 e^{LM^{(1)}}(i\phi - 1)f_2(\phi)\right\}\mathrm{d}\phi} \right]$$
$$\times \left(\frac{2}{S_0^2 e^{2LM^{(1)}}}\right), \tag{17}$$

where $\Re$ denotes the real part of a number,

$$f_{1,2}(\phi) = \exp(C_{1,2} + D_{1,2}V_0 + i\phi S_t),$$

$$C_{1,2} = ri\phi\tau + \frac{\kappa\theta}{\sigma^2}\left\{(b_{1,2} - \rho\sigma i\phi - d_{1,2})\tau - 2\log\left(\frac{1 - c_{1,2}e^{-d_{1,2}\tau}}{1 - c_{1,2}}\right)\right\},$$

$$D_{1,2} = \frac{(b_{1,2} - \rho\sigma i\phi - d_{1,2})}{\sigma^2}\left(\frac{1 - e^{-d_{1,2}\tau}}{1 - c_{1,2}e^{-d_{1,2}\tau}}\right),$$

$$\frac{\partial C_{1,2}}{\partial t} = ri\phi + \frac{\kappa\theta}{\sigma^2}\left\{(b_{1,2} - \rho\sigma i\phi + d_{1,2}) + 2\left(\frac{g_{1,2}d_{1,2}e^{d_{1,2}t}}{1 - g_{1,2}e^{d_{1,2}t}}\right)\right\},$$

$$\frac{\partial D_{1,2}}{\partial t} = \frac{(b_{1,2} - \rho\sigma i\phi + d_{1,2})}{\sigma^2}\left(\frac{d_{1,2}e^{d_{1,2}t}(g_{1,2}e^{d_{1,2}t})^{-1} + (1 - e^{d_{1,2}t})g_{1,2}d_{1,2}e^{d_{1,2}t}}{(1 - g_{1,2}e^{d_{1,2}t})^2}\right),$$

$$d_{1,2} = \sqrt{(\rho\sigma i\phi - b_{1,2})^2 - \sigma^2(2u_{1,2}i\phi - \phi^2)}, \quad c_{1,2} = \frac{b_{1,2} - \rho\sigma i\phi - d_{1,2}}{b_{1,2} - \rho\sigma i\phi + d_{1,2}}$$

$$b_1 = \kappa - \rho\sigma, \quad b_2 = \kappa, \quad u_1 = 0.5, \quad u_2 = -0.5.$$

Proof. See Appendix 5.3. $\qquad\square$

2.2   A Monte-Carlo approach

Alternatively, the conditional expectation in (11) can be computed using Monte-Carlo simulations. The simulations are performed using the Heston model and the calibrated parameters obtained minimizing the squared difference between theoretical Heston prices $C^\Theta(K,\tau)$ obtained from the model and observed market prices $C^M(K,\tau)$,

$$\min_{\Theta\in\mathbb{R}^5}\sum_{i=1}^{N}\left(C_i^\Theta(K_i,\tau_i) - C_i^M(K_i,\tau_i)\right) \tag{18}$$

where $\Theta \overset{\text{def}}{=} (\kappa, \theta, \sigma, v_0, \rho)$ Heston parameters, N number of options used for calibration, K strikes and τ times-to-maturity. Theoretical prices $C^\Theta(K, \tau)$ are obtained via numeric integration of the Heston characteristic function. The estimation results on day 20160205 for the SCO LETF yield $\widehat{\kappa} = 2.50$, $\widehat{\theta} = 0.53$, $\widehat{\sigma} = 1.32$, $\widehat{v}_0 = 1.41$, $\widehat{\rho} = 0.48$.

The Monte-Carlo algorithm is motivated by van der Stoep et al. (2014) and can be formulated as follows:

1. Generate N pairs of observations (s_i, v_i), $i = 1, \ldots, N$.

2. Order the realizations s_i: $s_1 \leq x_2 \leq \ldots \leq s_N$.

3. Determine the boundaries of M bins $(l_k, l_{k+1}]$, $k = 1, \ldots, M$ on an equidistant grid of values $S^* \overset{\text{def}}{=} S_0 e^{LM^{(1)}}$

4. For the kth bin approximate the conditional expectation (3) by

$$\mathsf{E}^{\mathsf{Q}}\left(\int_0^T \sigma_s^2 ds \,|\, S_T \in (l_k, l_{k+1}]\right) \approx \frac{h}{NQ(k)} \sum_{i=1}^{H} \sum_{j \in \mathcal{J}_k} V_{ij}, \qquad (19)$$

where h is the discretization step for V_t, $\mathcal{J}_k$ the set of numbers j, for which the observations S_T are in the kth bin and $Q(k)$ is the probability of S_T being in the kth bin.

The results of the simulation are presented in Figure 9. Polynomial smoothing is applied to produce the smoothed version of SCO LETF integrated volatility. The generated expected integrated variance has the form of a "smile" which confirms the intuition behind using average square implied volatility in the case of constant-volatility moneyness scaling approach.

3 Dynamic option trading strategy

3.1 The dynamic semiparametric factor model setup

3.1.1 Model description

A generalized version of the model in (6) represented by (7) assumes the implied volatility Y_t to be a stochastic process driven by a latent stochastic factor process $\mathcal{Z}_t$ contaminated by noise ε_t. To be more specific, define $\mathcal{J} \stackrel{\text{def}}{=} [\kappa_{min}, \kappa_{max}] \times [\tau_{min}, \tau_{max}]$, $Y_{t,j}$ implied volatility, $t = 1, \ldots, T$ time index, $j = 1, \ldots, J_t$ option intraday numbering on day t, $X_{t,j} \stackrel{\text{def}}{=} (\kappa_{t,j}, \tau_{t,j})^\top$, $\kappa_{t,j}$, $\tau_{t,j}$ are, respectively, a moneyness measure (log-, forward, etc.) and time-to-maturity at time point t for option j. Then the *dynamic semiparametric factor model (DSFM)* is defined as follows: assume

$$Y_{t,j} = \mathcal{Z}_t^\top m(X_{t,j}) + \varepsilon_{t,j}, \tag{20}$$

where $\mathcal{Z}_t = (1, Z_t^\top)$, $Z_t = (Z_{t,1}, \ldots, Z_{t,L})^\top$ unobservable L-dimensional stochastic process, $m = (m_0, \ldots, m_L)^\top$, real-valued functions; m_l, $l = 1, \ldots, L+1$ are defined on a subset of $\mathbb{R}^d$. The full description of the model is given in Park et al. (2009). One can estimate:

$$\widehat{Y}_t = \widehat{\mathcal{Z}}_t^\top \widehat{m}(X_t) \tag{21}$$

$$= \widehat{\mathcal{Z}}_t^\top \widehat{\mathcal{A}} \psi(X_t), \tag{22}$$

with $\psi(X_t) \stackrel{\text{def}}{=} \{\psi_1(X_t), \ldots, \psi_K(X_t)\}^\top$ being a space basis such as a tensor B-spline basis, $\mathcal{A}$ is the $(L+1) \times K$ coefficient matrix. In this case K denotes the number of tensor B-spline sites: let $(s_u)_{u=1}^U$, $(s_v)_{v=1}^V$ be the B-spline sites for moneyness and

time-to-maturity coordinates, respectively, then $K = U \cdot V$. Given some spline orders n_κ and n_τ for both coordinates and sets of knots $(t_i^\kappa)_{i=1}^M$, $(t_j^\tau)_{j=1}^N$, one of the Schoenberg-Whitney conditions requires that $U = M - n_\kappa$, $V = N - n_\tau$, see De Boor (2001). The usage of the parameter K is roughly analogous to the bandwidth choice in Fengler et al. (2003) and Fengler et al. (2007); however the results of Park et al. (2009) demonstrate insensitivity of DSFM estimation results to the choice of K, n.

The estimates for the IV surfaces $\widehat{m}_l$ are re-calculated on a fine 2-dimensional grid of tensor B-spline sites: the estimated coefficient matrix $\widehat{\mathcal{A}}$ is reshaped into a $U \times V \times L + 1$ array of $L + 1$ matrices $\widehat{A}$ of dimension $U \times V$. Factor functions m_l can then be estimated as follows:

$$\widehat{m}_{l;i,j} = \sum_i^U \sum_j^V \widehat{A}_{l;i,j} \psi_{i,k_\kappa}(\kappa_i) \psi_{j,k_\tau}(\tau_j), \tag{23}$$

where k_κ, k_τ are knot sequences for the moneyness and time-to-maturity coordinates, respectively.

The estimated factor functions $\widehat{m}_l$ together with stochastic factor loadings $\widehat{\mathcal{Z}}_t$ are combined into the dynamic estimator of the implied volatility surface:

$$\widehat{IV}_{t;i,j} = \widehat{m}_{0;i,j} + \sum_{l=1}^L \widehat{\mathcal{Z}}_{l,t} \widehat{m}_{l;i,j}, \tag{24}$$

can be modeled as a vector autoregressive process. It should be noted that $\widehat{m}_l$ and $\widehat{\mathcal{Z}}_{l,t}$ are not uniquely defined, so an orthonormalization procedure must be applied.

An indication of possible mispricing of LETF options allows to test an investment strategy based on the comparison of the theoretical price obtained from the moneyness scaling correction as well as the application of the DSFM model and the market

price. Such a strategy would mainly exploit the two essential elements of information from these two approaches. The first element is obtaining an indication of arbitrage opportunities resulting from the mismatch between ETF and LETF IVs. The moneyness scaling approach allows to estimate LETF IV using richer unleveraged ETF data which also would make the DSFM IV estimator more consistent. The second element is implied volatility forecasting. The DSFM model allows to forecast a whole IV surface via the dynamics of stochastic factor loadings $\mathcal{Z}_t$.

3.1.2 Empirical results

For the model's empirical testing, we use the data on SPY and SSO (L)ETF European call options in the period 20140920-20150630. The data summary statistics are outlined in Table 1 below.

To avoid computational problems, the estimation space $[\kappa_{min}, \kappa_{max}] \times [\tau_{min}, \tau_{max}]$ for covariates $X_t = (\kappa_t, \tau_t)^\top$, which covers in (forward) moneyness $\kappa \in [0.3, 1.5]$ and in time-to-maturity $\tau \in [0.3, 1.0]$, is re-scaled (via marginal distribution functions) to $[0, 1]^2$. The model is estimated using numerical methods, see Park et al. (2009). The number of the dynamic functions has to be chosen in advance. One should also notice that for m_l to be chosen as eigenfunctions of the covariance operator $K(u, v) \stackrel{\text{def}}{=} \text{Cov}\{Y(u), Y(v)\}$ in an L-dimensional approximating linear space, where Y is understood to be the random IV surface, they should be properly normalized, such that $\|m_l(\cdot)\| = 1$ and $\langle m_l, m_k \rangle = 0$ for $l \neq k$.

The choice of L can be based on the explained variance by factors:

$$EV(L) \stackrel{\text{def}}{=} 1 - \frac{\sum_{t=1}^{T} \sum_{j=1}^{J_t} \left\{ Y_{t,j} - \sum_{l=0}^{L} \widehat{Z}_{t,l} \widehat{m}_l(X_{t,j}) \right\}^2}{\sum_{t=1}^{T} \sum_{j=1}^{J_t} (Y_{t,j} - \overline{Y})^2} \tag{25}$$

The model's goodness-of-fit is evaluated by the root mean squared error (RMSE) criterion:

$$RMSE \overset{\text{def}}{=} \sqrt{\frac{1}{\sum_t J_t} \sum_{t=1}^{T} \sum_{j=1}^{J_t} \left\{ Y_{t,j} - \sum_{l=0}^{L} \widehat{Z}_{t,l} \widehat{m}_l(X_{t,j}) \right\}^2} \qquad (26)$$

The $EV(L)$ and $RMSE$ criteria are displayed in Table 2 below. The model order $L = 3$ is chosen for model estimation. The data for the SPY ETF option are used with parameters $n_\kappa, n_\tau = 3$; $M = 9$, $N = 7$, so that $U = 6$, $V = 4$, $K = 6 \cdot 4 = 24$. The estimates for the factor functions m_l according to (23) are plotted in Figure 11 below. Furthermore, we can study the statistical properties of the stochastic factor loadings $\widehat{\mathcal{Z}}_t$ estimated by the model. Figure 10 shows the dynamics of $\widehat{\mathcal{Z}}_t$ in time. Significant "spikes" in the beginning of the period correspond to the period of relatively large values of the VIX index. The first of them happen before the largest increase in the VIX values in the given period, therefore the model has predictive value with respect to market instability dynamics.

Theoretical and simulation results in Park et al. (2009) justify using vector autoregression (VAR) analysis to model $\widehat{\mathcal{Z}}_t$. To select a VAR model, we computed the Schwarz (SC), the Hannan-Quinn (HQ) and the Akaike (AIC) criteria, as shown in Table 3. All three criteria select the VAR(1) model. Furthermore, the roots of the characteristic polynomial all lie inside the unit circle, which shows that the specified model is stationary. Portmanteau and Breusch-Godfrey LM test results with 12 lags for the autocorrelations of the error term fail to reject residual autocorrelation at 10% significance level.

The estimates of factor functions, stochastic loadings $\widehat{m}_l$, $\widehat{\mathcal{Z}}_t$ together determine the dynamics of implied volatility surfaces $\widehat{IV}_t$, as in (24). As an illustration, both the observed IV "strings" and the fitted by DSFM IV surface are displayed in Figure 12.

16

The degenerate nature of implied volatility data is reflected by the fact that empirical observations do not cover estimation grids at given time points. This is due to the fact that contracts at certain maturities or strikes are not always traded. The DSFM fitting procedure introduces basis functions which approximate a high-dimensional space and depend on time. This allows to account for all information in the dataset simultaneously in one minimization procedure which runs over all $\widehat{m}_l$ and $\widehat{\mathcal{Z}}_t$ and avoid bias problems which would inevitably occur if some kernel smoothing procedure such as Nadaraya-Watson were applied for this type of degenerate data.

3.2 The strategy

3.2.1 Description

Ability to forecast the whole surface of implied volatility can be used in combination with the moneyness scaling technique to exploit potential discrepancies in ETF and LETF option prices or implied volatilities to build an arbitrage trading strategy. A suitable strategy would be the so-called "trade-with-the-smile/skew" strategy adapted for the special case of ETF-LETF option IV discrepancy. It would use the ETF option data to estimate the model (theoretical) smile of the leveraged counterpart and the information from the IV surface forecast to recognize the future (one-period-ahead) possible IV discrepancy.

Going back to the results in Section 1.2, one can come to a conclusion that there's a certain discrepancy between SPY and SSO option implied volatilities from the statistical point of view, so we consider these two options in the strategy setup. The strategy can be outlined as follows: choose a moving window width w; then for each $t = w, \ldots, T$, T is the final time point in the sample do the following:

1. Given two leverage ratios $\beta_2 = 1$, β_1, re-scale the log-moneyness coordinate LM^{β_2} according to the moneyness scaling formula (3) to obtain $\widehat{LM}^{\beta_1}$. This will be the "model" moneyness coordinate for DSFM estimation.

2. Estimate the DSFM model (20) on the space $[\widehat{LM}_{min}^{\beta_1}, \widehat{LM}_{max}^{\beta_1}] \times [\tau_{min}^{SPY}, \tau_{max}^{SPY}]$ (re-scaled to $[0,1]^2$, as suggested above). This will yield the IV surface estimates $\widehat{IV}_1, \ldots, \widehat{IV}_t$.

3. Forecast the IV surface estimate $\widehat{IV}_{t+1}$ using the VAR structure of the estimated stochastic loadings $\hat{\mathcal{Z}}_t$ and factor functions $\widehat{m}_l$.

4. Choose a specific IV "string" for some time-to-maturity τ^* at time point t using SSO option data and calculate the marginally transformed value $\widehat{LM}_{\tau^*}^{\beta_1}$ of the *true* SSO log-moneyness LM^{β_1} using the marginal distribution of $\widehat{LM}^{\beta_1}$.

5. Using $\widehat{LM}_{\tau^*}^{\beta_1}$, τ^* and $\widehat{IV}_{t+1}$, interpolate the "theoretical" IV $\widehat{IV}_{t+1}$ over the marginally re-scaled $[\widehat{LM}_{min}^{\beta_1}, \widehat{LM}_{max}^{\beta_1}] \times [\tau^*, \tau^*]$ to obtain "theoretical" values $\widehat{IV}_{t+1;LM_{\tau^*}^{\beta_1}, \tau^*}$.

6. Compare "theoretical" values $\widehat{IV}_{t+1;LM_{\tau^*}^{\beta_1}, \tau^*}$ with "true" $IV_{t;LM_{\tau^*}^{\beta_1}, \tau^*}$ and construct a delta-hedged option portfolio:

   - if $\widehat{IV}_{t+1;LM_{\tau^*}^{\beta_1}, \tau^*} > IV_{t;LM_{\tau^*}^{\beta_1}, \tau^*}$ for the whole $LM_{\tau^*}^{\beta_1}$, then buy (long) options corresponding to the largest difference $\widehat{IV}_{t+1;LM_{\tau^*}^{\beta_1}, \tau^*} - IV_{t;LM_{\tau^*}^{\beta_1}, \tau^*}$

   - if $\widehat{IV}_{t+1;LM_{\tau^*}^{\beta_1}, \tau^*} < IV_{t;LM_{\tau^*}^{\beta_1}, \tau^*}$ for the whole $LM_{\tau^*}^{\beta_1}$, then sell (short) options corresponding to the largest difference $IV_{t;LM_{\tau^*}^{\beta_1}, \tau^*} - \widehat{IV}_{t+1;LM_{\tau^*}^{\beta_1}, \tau^*}$

   - if $\widehat{IV}_{t+1;LM_{\tau^*}^{\beta_1}, \tau^*}$ and $IV_{t;LM_{\tau^*}^{\beta_1}, \tau^*}$ intersect, then buy (long) an option with the absolute largest negative deviation from the "theoretical" IV (IV expected to fall) and sell (short) an option with the smallest positive deviation from

the "theoretical" IV (IV expected to increase). In all three cases use the underlying SSO LETF asset to make the whole portfolio delta-neutral.

7. At time point $t+1$, terminate the portfolio, calculate profit/loss and repeat until time T.

The strategy described above aims to exploit the information from the discrepancies between the forecast "theoretical" (model) SSO LETF implied volatilities and the historical ("true") ones. It protects the portfolio against unfavorable moves in the underlying asset L_t through delta-hedging and aims to gain from forecast moves in another option risk factor, the implied volatility via its explicit estimation and forecasting. The basic strategy presented here can be extended in several ways: further, including higher-order, option price sensitivities may be accounted for, such as gamma, theta hedging or charm-adjusted delta hedging. The amounts of bought and sold options can also be adjusted according to investor risk and return profiles and preferences.

3.2.2 Empirical application

Steps 2 and 3 of the dynamic strategy described above involve estimation out-of-sample forecasting of the IV surface $\widehat{IV}_{t+1}$ using the model estimates. The model parameters are taken to be the same as in Section 3.1.2. The rolling window width is 100 and the forecasting horizon is 1 day ahead. The prediction quality at time point $t+1$ is measured by the root mean squared prediction error (RMSPE) given by

$$RMSPE \stackrel{\text{def}}{=} \sqrt{\frac{1}{J_{t+1}} \sum_{j=1}^{J_{t+1}} \left\{ Y_{t+1,j} - \sum_{l=0}^{L} \widehat{Z}_{t+1,l} \widehat{m}_l(X_{t+1,j}) \right\}^2} \tag{27}$$

The starting point of rolling-window estimation of the strategy is 20150415. The

plot in Figure 13 below shows the RMSPE measure in time for three different model orders: $L = 2, 3, 4$. The average RMSPEs for $L = 2, 3, 4$ are, respectively, 0.095, 0.096 and 0.099; they decrease slightly as the order increases which reflects a well-known finding that more parsimonious models perform better in forecasting, see Zellner et al. (2002).

The dynamic strategy performance in the period 20150415-20150701 is displayed in Figure 14. Out of 55 investment periods, in 13 periods long portfolios were constructed, the remaining 42 periods net short positions were taken. The strategy is a self-financing strategy: no exogenous money infusions are done in its whole course. Furthermore, the potential of this strategy is even higher than displayed because only a fraction of already accumulated total proceeds was invested continuously following the simple setup in 3.2.1, where only two options were included into the portfolio each time. The presented strategy correctly guessed the direction of SSO LETF IV moves 82% of times.

4   Conclusions

In this paper, we study the statistical properties of the moneyness scaling transformation by Leung and Sircar (2015). This transformation adjusts the moneyness coordinate of the implied volatility smile in an attempt to remove the discrepancy between the IV smiles for levered and unlevered ETF options. We construct bootstrap uniform confidence bands which indicate that in a statistical sense there remains a possibility that the implied volatility smiles are still not the same, even after moneyness scaling has been performed. This presents possible arbitrage opportunities on the (L)ETF market which can be exploited by traders.

We propose a stochastic volatility approach which aims to improve the accuracy of the moneyness scaling method by explicit estimation of the conditional expectation of integrated stochastic volatility. We present two approaches to implement this estimate: via semi-analytic calculation based on Fourier transforms and by means of a Monte-Carlo method.

A dynamic "trade-with-the-smile" strategy based on a dynamic semiparametric factor model is presented. This strategy utilizes the dynamic structure of implied volatility surface allowing out-of-sample forecasting and information on unleveraged ETF options to construct theoretical one-step-ahead implied volatility surfaces. The proposed strategy has the potential to generate significant trading gains due to simultaneous use of the information from the discrepancies between the forecast "theoretical" (model) SSO LETF implied volatilities and the historical ("true") ones. It protects the portfolio against unfavorable moves in the underlying asset through delta-hedging and aims to gain from forecast moves in another option risk factor, the implied volatility via its explicit estimation and forecasting via an advanced statistical model.

List of Figures

References

Aït-Sahalia, Y., Bickel, P. J., Stoker, T. M. (2001): "Goodness-of-fit tests for kernel regression with an application to option implied volatilities", *Journal of Econometrics*, **105(2)**, 363–412

de Boor, C. (2001): "A Practical Guide to Splines. Revised Edition", *Springer*

Berument, H., Kiymaz, H. (2001): "The day of the week effect on stock market volatility", *Journal of Economics and Finance*, **25(2)**, 181–193

Charles, A. (2010): "The day-of-the-week effects on the volatility: The role of the asymmetry", *European Journal of Operational Research*, **202(1)**, 143–152

Cont, R., da Fonseca, J. (2002): "Dynamics of implied volatility surfaces", *Quantitative Finance*, **2(1)**, 45–60

Dragulescu, A. and Yakovenko, V. (2002): "Probability distribution of returns in the Heston model with stochastic volatility", *Quantitative Finance*, **2**, 443–453

Fengler, M. R., Härdle, W. K., Villa, C. (2003): "The dynamics of implied volatilities: a common principal components approach", *Review of Derivatives Research*, **6**, 179–202

Fengler, M. R., Härdle, W. K., & Mammen, E. (2007): "A semiparametric factor model for implied volatility surface dynamics", *Journal of Financial Econometrics*, **5(2)**, 189–218

Franke, J., Härdle, W., & Hafner, C. (2015): "Statistics of Financial Markets: An Introduction", *Springer, 4th edition*

Hall, P., Horowitz, J. (2013): "A simple bootstrap method for constructing nonparametric confidence bands for functions", *The Annals of Statistics*, **41(4)**, 1892–1921

Härdle, W. (1989): "Asymptotic maximal deviation of M-Smoothers", *Journal of Multivariate Analysis*, **29**, 163–179

Härdle, W. (1990): "Applied Nonparametric Regression", *Cambridge University Press*

Härdle, W. K., Ritov, Y., Wang, W. (2015): "Tie the straps: uniform bootstrap confidence bands for semiparametric additive models", *Journal of Multivariate Analysis*, **134**, 129–145

Heston, S. L. (1993): "A closed-form solution for options with stochastic volatility with applications to bond and currency options", *The Review of Financial Studies*, **6**, 327–343

Huber, P. J. (1964): "Robust estimation of a location parameter", *Annals of Mathematical Statistics*, **35(1)**, 73–101

Hull, J. C. and White, A. (1987): "The pricing of options on assets with stochastic volatilities", *Journal of Finance*, **42**, 281–300

Lakonishok, J., Smidt, S. (1988): "Are seasonal anomalies real? A ninety-year perspective", *The Review of Financial Studies*, **1(4)**, 403–425

Leung, T., Sircar, R. (2015): "Implied volatility of leveraged ETF options", *Applied Mathematical Finance*, **22(2)**, 162–188

Park, B. U., Mammen, E., Härdle, W., Borak, S. (2009): "Time Series Modelling With Semiparametric Factor Dynamics", *Journal of the American Statistical Association*, **104(485)**, 284–298

Rouah, F. (2013): "The Heston model and its extensions in Matlab and C#", *Wiley*

Ruppert, D., Wand, M. P. (1994): "Multivariate locally weighted least squares regression", *The annals of statistics*, **22(3)**, 1346–1370

Schöbel, R. and Zhu, J. (1999): "Stochastic Volatility With an Ornstein-Uhlenbeck Process: An Extension", *European Finance Review*, **3**, 24–46

van der Stoep, A. W., Grzelak, L. A., Oosterlee, C. W. (2014): "The Heston stochastic-local volatility model: efficient Monte-Carlo simulation", *International Journal of Theoretical and Applied Finance*, **17(7)**, 1–30

Zellner, A., Keuzenkamp, H. A., McAleer, M. (2002): "Simplicity, inference and modelling", *Cambridge University Press*

5 Appendix

5.1 Moneyness scaling formula

Given the asset (S&P 500) price dynamics

$$\frac{dS_t}{S_t} = r dt + \sigma dW_t^{\mathsf{Q}} \tag{28}$$

with interest rate r and volatility σ; W_t^{Q} standard Brownian motion under the risk-neutral measure Q, the (L)ETF dynamics is given by:

$$\begin{aligned}
\frac{dL_t}{L_t} &= \beta \left(\frac{dS_t}{S_t} \right) - \{(\beta - 1)r + c\}dt \\
&= (r - c)dt + \beta \sigma dW_t^{\mathsf{Q}},
\end{aligned} \tag{29}$$

26

where $0 \leq c \ll r$ is the (L)ETF expense ratio (approximates an annual fee charged by the ETF from the shareholders to cover the fund's operating expenses). Then the general solution of (29) is given by:

$$L_T = L_t \exp\left\{(r - c)(T - t) - \frac{\beta^2}{2} \int_t^T \sigma_s^2 ds + \beta \int_t^T \sigma_s dW_s^{\mathsf{Q}}\right\}. \tag{30}$$

If we write (30) for $L_T^{(\beta_1)}$, $L_T^{(\beta_2)}$, we obtain

$$\frac{L_T^{(\beta_1)}}{e^{(r-c)\tau} L_t^{(\beta_1)}} = \exp\left(-\frac{\beta_1^2}{2} \int_0^\tau \sigma_s^2 ds + \beta_1 \int_0^\tau \sigma_s dW_s^{\mathsf{Q}}\right), \tag{31}$$

$$\frac{L_T^{(\beta_2)}}{e^{(r-c)\tau} L_t^{(\beta_2)}} = \exp\left(-\frac{\beta_2^2}{2} \int_0^\tau \sigma_s^2 ds + \beta_2 \int_0^\tau \sigma_s dW_s^{\mathsf{Q}}\right), \tag{32}$$

where σ_s is the instantaneous volatility at time s.

From (32) it follows:

$$\int_t^T \sigma_s dW_s^{\mathsf{Q}} = \frac{\log\left(\frac{L_T^{(\beta_2)}}{e^{(r-c)\tau} L_t^{(\beta_2)}}\right) + \frac{\beta_2^2}{2} \int_0^\tau \sigma_s^2 ds}{\beta_2}. \tag{33}$$

Substitute (33) into (31) to eliminate the stochastic term $\int_t^T \sigma_s dW_s^{\mathsf{Q}}$ and obtain:

$$\frac{L_T^{(\beta_1)}}{e^{(r-c)\tau} L_t^{(\beta_1)}} = \exp\left\{-\frac{\beta_1}{2}(\beta_1 - \beta_2) \int_0^\tau \sigma_s^2 ds\right\} \left\{\frac{L_T^{(\beta_2)}}{e^{(r-c)\tau} L_t^{(\beta_2)}}\right\}^{\frac{\beta_1}{\beta_2}} \tag{34}$$

Now take logarithms and expectations conditioned on $K^{(\beta_1)} = L_T^{(\beta_1)}$ and $K^{(\beta_2)} = L_T^{(\beta_2)}$

and obtain:

$$\log(k_f{}^{(\beta_1)}) = -\frac{\beta_1}{2}(\beta_1 - \beta_2)\mathsf{E}^{\mathsf{Q}}\left(\int_0^\tau \sigma_s^2 \mathrm{d}s \,\middle|\, K^{(\beta_1)} = L_T^{(\beta_1)}, K^{(\beta_2)} = L_T^{(\beta_2)}\right)$$
$$+\frac{\beta_1}{\beta_2}\log(k_f{}^{(\beta_2)})$$

Assuming constant σ and exponentiating, one obtains (5).

5.2   The local linear M-smoothing estimator

M-type smoothers apply a nonquadratic loss function $\rho(\cdot)$ to make estimation more robust. Given the model

$$Y_i = m(X_i) + \varepsilon_i, \tag{35}$$

where $Y_i \in \mathbb{R}$, $X_i \in \mathbb{R}^d$, $\varepsilon_i \stackrel{\text{def}}{=} \sigma(X_i)u_i$, $u_i \sim (0,1)$, iid, $\mathcal{X} \stackrel{\text{def}}{=} \{(X_i, Y_i); 1 \le i \le n\}$, the local linear M-smoothing estimator is obtained from:

$$\min_{\alpha \in \mathbb{R}, \beta \in \mathbb{R}^p} \sum_{i=1}^n \rho\left\{Y_i - \alpha - \beta^\top(X_i - x)\right\} W_{ih}(x), \tag{36}$$

where

$$W_{hi}(x) \stackrel{\text{def}}{=} \frac{h^{-2}K'\{(x - X_i)/h\}}{\widehat{f}_h(x)} - \frac{K_h(x - X_i)\widehat{f}_h'(x)}{\widehat{f}_h^2(x)} \tag{37}$$

is a kernel weight sequence with $\widehat{f}_h'(x) \stackrel{\text{def}}{=} n^{-1}\sum_{i=1}^n K_h'(x - X_i)$, h is the bandwidth, K is a kernel function; $\int K(u)du = 1$, $K_h(\cdot) \stackrel{\text{def}}{=} h^{-1}K(\cdot/h)$. The function $\rho(\cdot)$ is designed to provide more robustness than the quadratic loss. An example of such a function is given by Huber (1964), see also Härdle (1989):

$$\rho(u) = \begin{cases} 0.5u^2, & \text{if } |u| \leq c; \\ c|u| - 0.5c^2 & \text{if } |u| > c. \end{cases} \tag{38}$$

with the constant c regulating the degree of resistance.

5.3 Proof of Proposition 2.1.1

The proof is based on the usage of the Dupire formula, which is a result from local volatility analysis. It is known that the Dupire formula allows to compute the local volatility of a European option, defined by

$$\sigma_{K,T}^2(S_t, t) \overset{\text{def}}{=} \mathbb{E}^{\mathbb{Q}}\{\sigma^2(S_T, T, t, \cdot)|S_T = K, \mathcal{F}_t\} \tag{39}$$

$$= \frac{\frac{\partial C}{\partial T}}{\frac{K^2}{2}\frac{\partial^2 C}{\partial K^2}} \tag{40}$$

Then, given the Heston setup, $\sigma^2(S_T, T, t, \cdot) = V_t$, some constant $LM^{(1)}$, it follows that

$$\mathbb{E}^{\mathbb{Q}}\left(\int_0^T V_t \mathrm{d}t \,\middle|\, \log\left(\frac{S_T}{S_0}\right) = LM^{(1)}\right) = \int_0^T \mathbb{E}^{\mathbb{Q}}\left(V_t \,\middle|\, \log\left(\frac{S_T}{S_0}\right) = LM^{(1)}\right) \mathrm{d}t$$

$$= \int_0^T \mathbb{E}^{\mathbb{Q}}\left(V_t \,\middle|\, S_T = S_0\exp(LM^{(1)})\right) \mathrm{d}t$$

$$= \int_0^T \mathbb{E}^{\mathbb{Q}}\left(V_t \,\middle|\, S_T = \widetilde{K}\right) \mathrm{d}t,$$

where $\widetilde{K}$ is some constant strike price for a european call option on the ETF X. Then applying the Dupire formula (40) to $\mathbb{E}^{\mathbb{Q}}\left(V_t \,\middle|\, S_T = \widetilde{K}\right)$ yields

$$\mathbb{E}^{\mathbb{Q}}\left(\int_0^T V_t \mathrm{d}t \,\bigg|\, \log\left(\frac{S_T}{S_0}\right) = LM^{(1)}\right) = \int_0^T \mathbb{E}^{\mathbb{Q}}\left(V_t \,\big|\, S_T = \widetilde{K}\right)\mathrm{d}t$$

$$= \frac{\frac{\partial C_H}{\partial T}}{\frac{\widetilde{K}^2}{2}\frac{\partial^2 C_H}{\partial \widetilde{K}^2}},$$

where C_H is the Heston price of the call option. The partial derivatives $\partial C_H/\partial T$ and $\partial^2 C_H/\partial \widetilde{K}^2$ are the "Heston Greeks" and are given, e.g., in Rouah (2013). After simplifications, one obtains (17).

6 Tables

		Min.	Max.	Mean	Stdd.	Skewn.	Kurt.
SPY	TTM	0.26	1.05	0.76	0.19	-0.54	2.76
	Moneyness	0.05	1.43	0.48	0.17	-0.34	3.15
	IV	0.25	1.55	0.46	0.23	1.94	7.17
SSO	TTM	0.21	1.04	0.63	0.25	0.01	1.76
	Moneyness	0.18	1.69	0.63	0.29	0.92	3.61
	IV	0.25	1.34	0.41	0.11	1.91	10.81

Table 1: *Summary statistics on SPY, SSO (L)ETF options from 20140920 to 20150630 (in total $\sum_t J_t = 9828, 7619$ datapoints, respectively). Source: Datastream*

Criterion	$L = 2$	$L = 3$	$L = 4$	$L = 5$
$EV(L)$	0.915	0.921	0.925	0.930
$RMSE$	0.090	0.088	0.087	0.082

Table 2: Explained variance and RMSE criteria for different model order sizes

Model order n	AIC(n)	HQ(n)	SC(n)
1	-4.20^*	-4.10^*	-3.96^*
2	-4.13	-3.96	-3.72
3	-4.07	-3.83	-3.48
4	-4.03	-3.72	-3.27
5	-3.97	-3.59	-3.03

Table 3: The VAR model selection criteria. The smallest value is marked by an asterisk

7   Figures
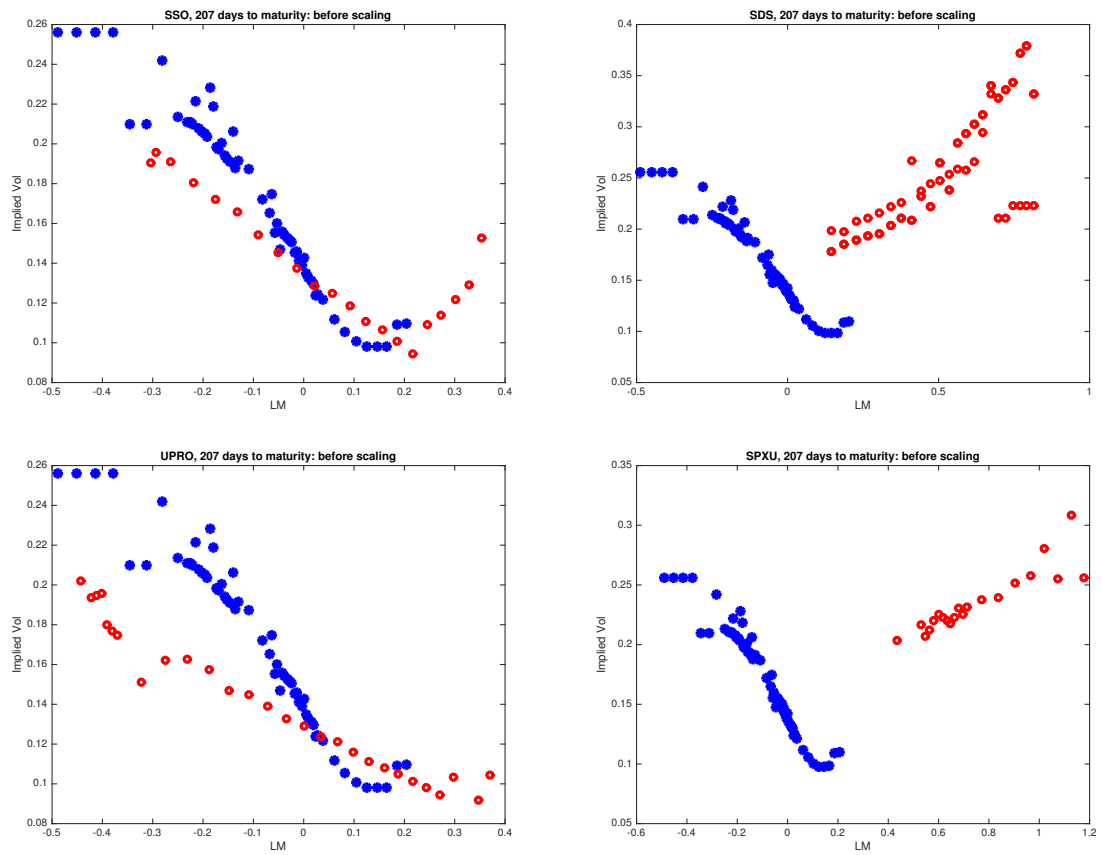
Figure 1: SPY (blue) and LETFs (red) implied volatilities before scaling on June 23, 2015 with 207 days to maturity, plotted against their log-moneyness

LETFIV
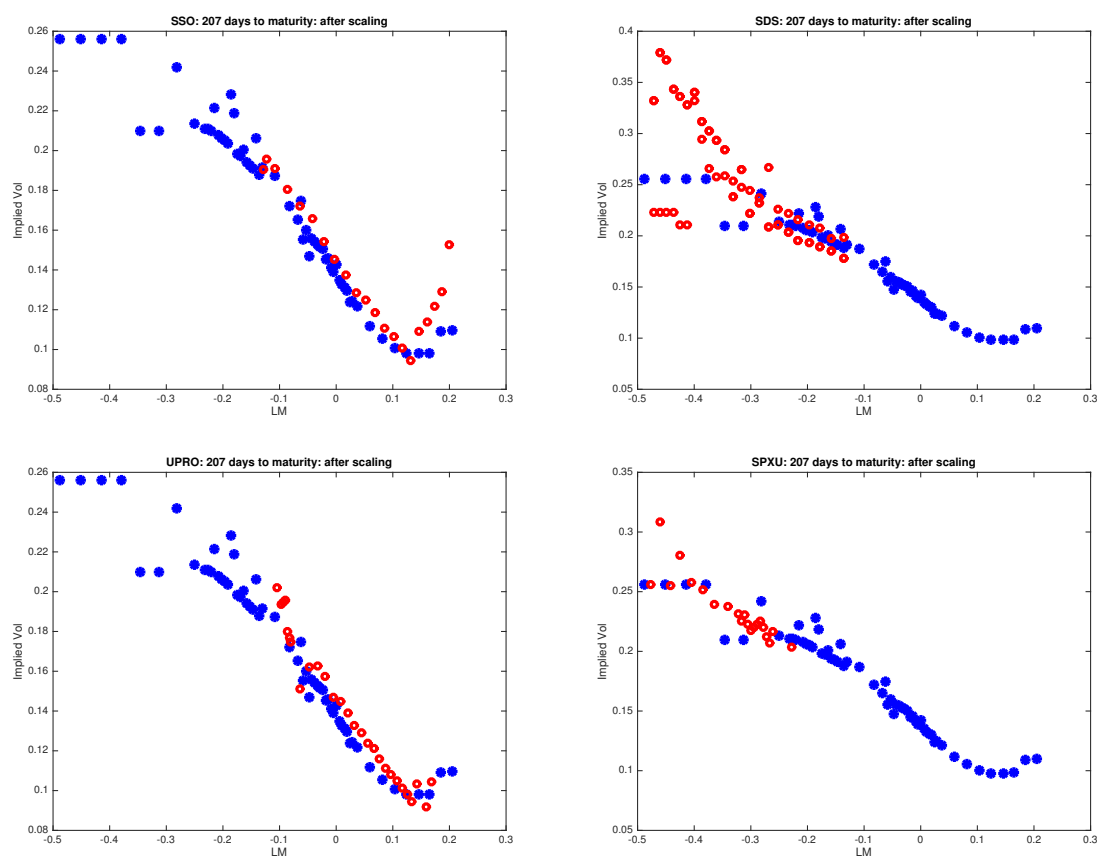
Figure 2: SPY (blue) and LETFs (red) implied volatilities after moneyness scaling on June 23, 2015 with 207 days to maturity, plotted against their log-moneyness

LETFIVMonSc
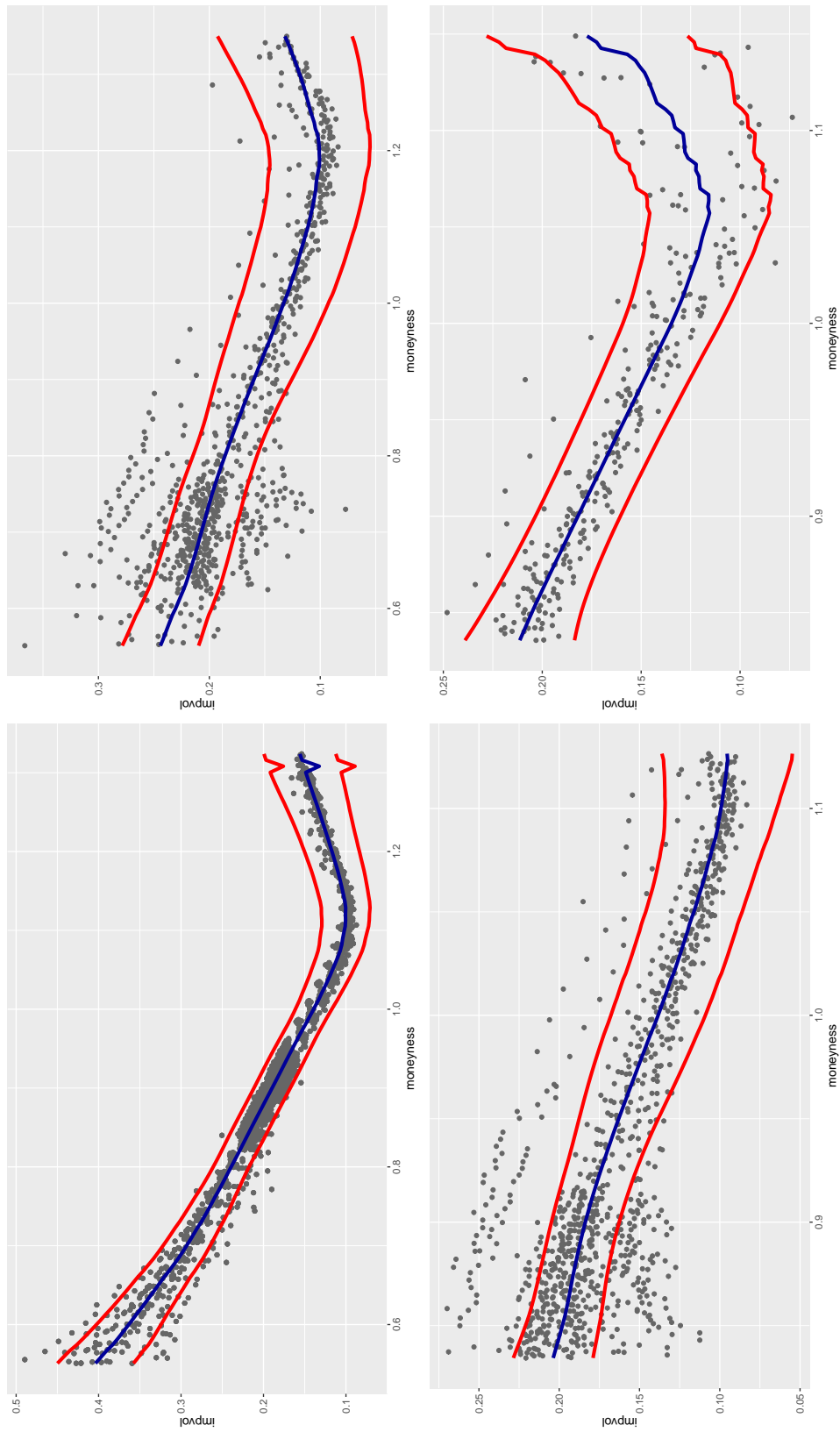
Figure 3: Fitted implied volatility and bootstrap uniform confidence bands for 4 (L)ETFs on S&P500; τ: 0.5 years

LETFConfBands05SPY   LETFConfBands05SSO   LETFConfBands05UPRO   LETFConfBands05SDS

34
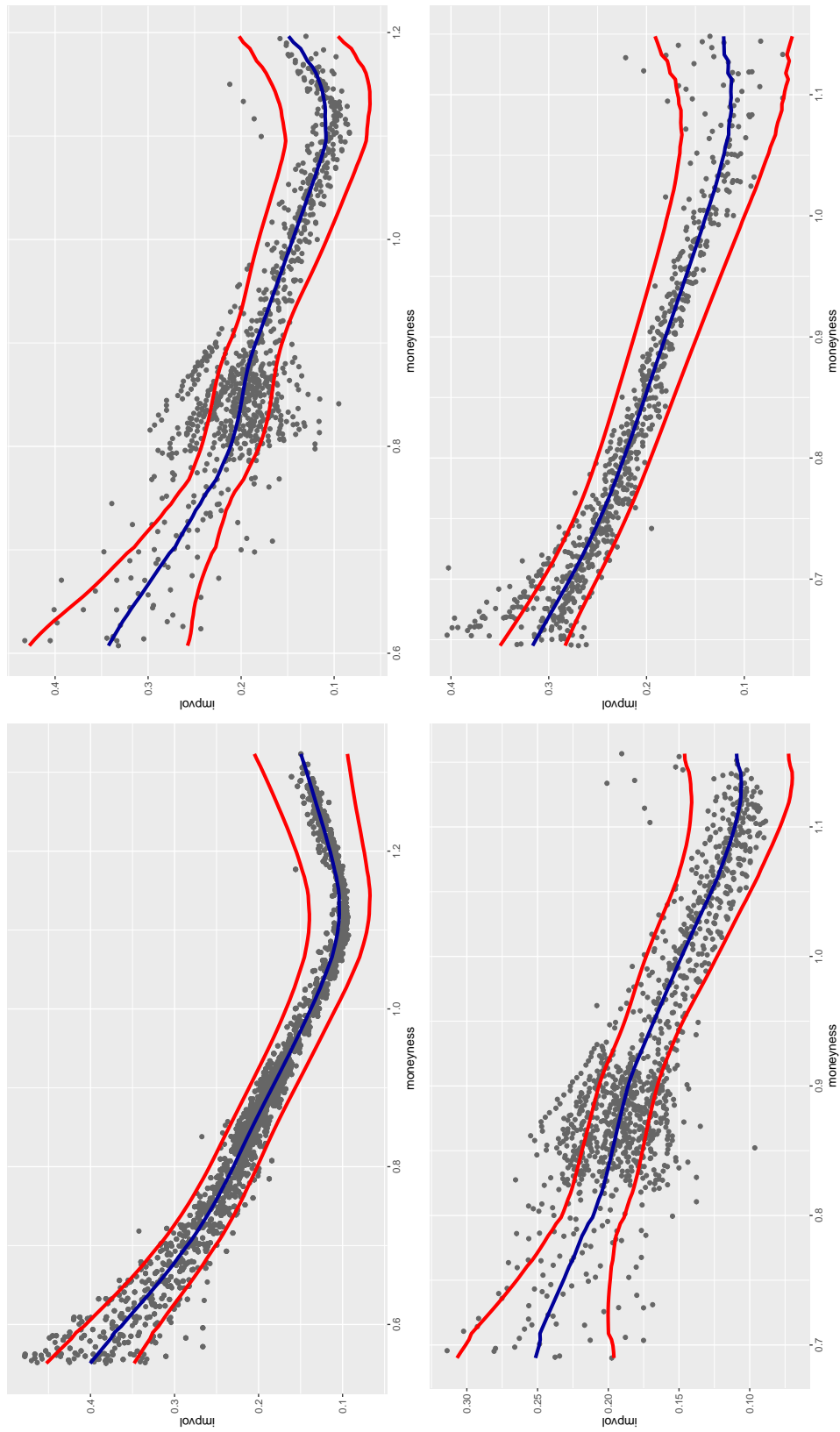
Figure 4: Fitted implied volatility and bootstrap uniform confidence bands for 4 (L)ETFs on S&P500; τ: 0.6 years

LETFConfBands06SPY   LETFConfBands06SSO   LETFConfBands06UPRO   LETFConfBands06SDS
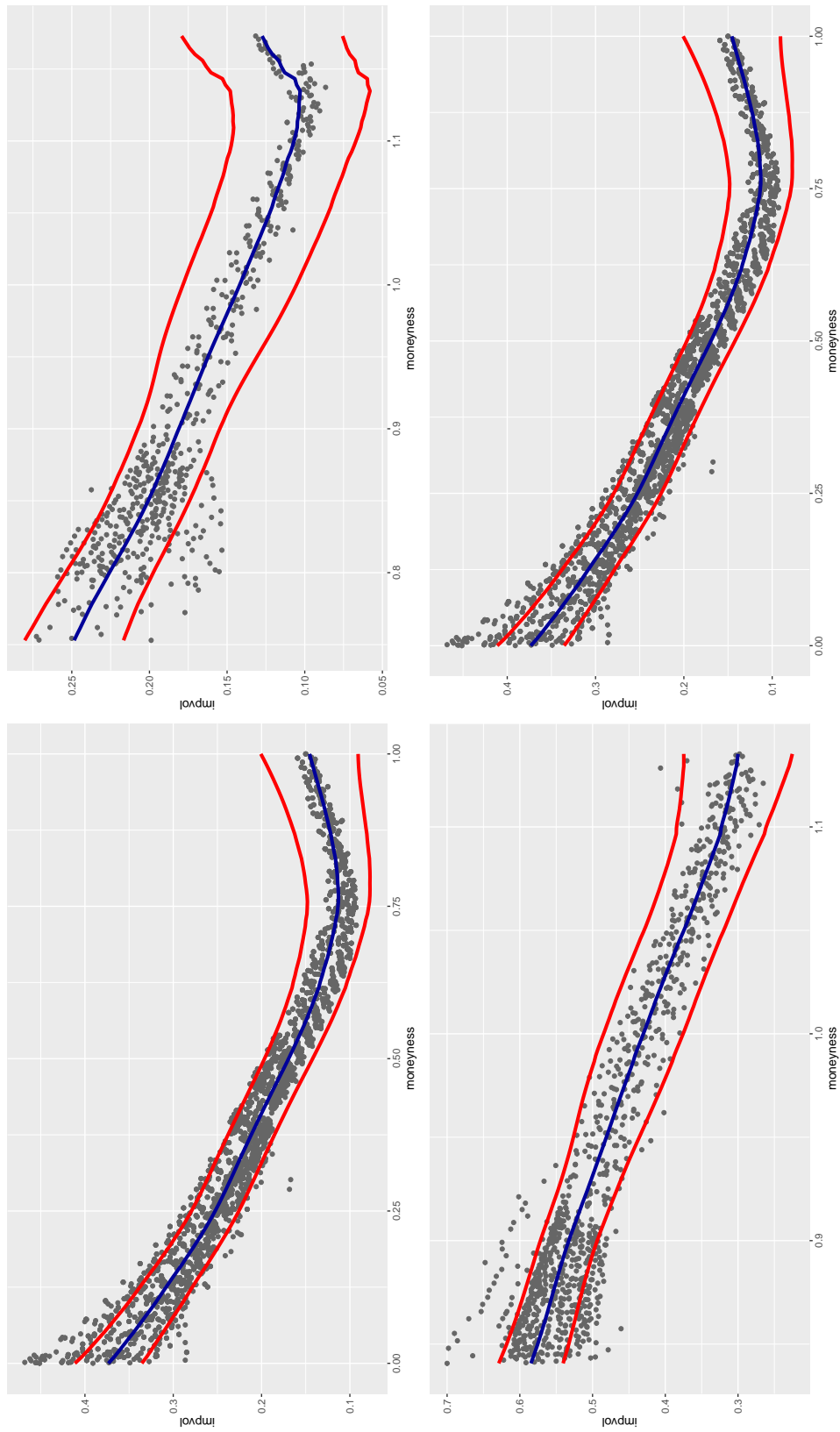
Figure 5: Fitted implied volatility and bootstrap uniform confidence bands for 4 (L)ETFs on S&P500; τ: 0.7 years
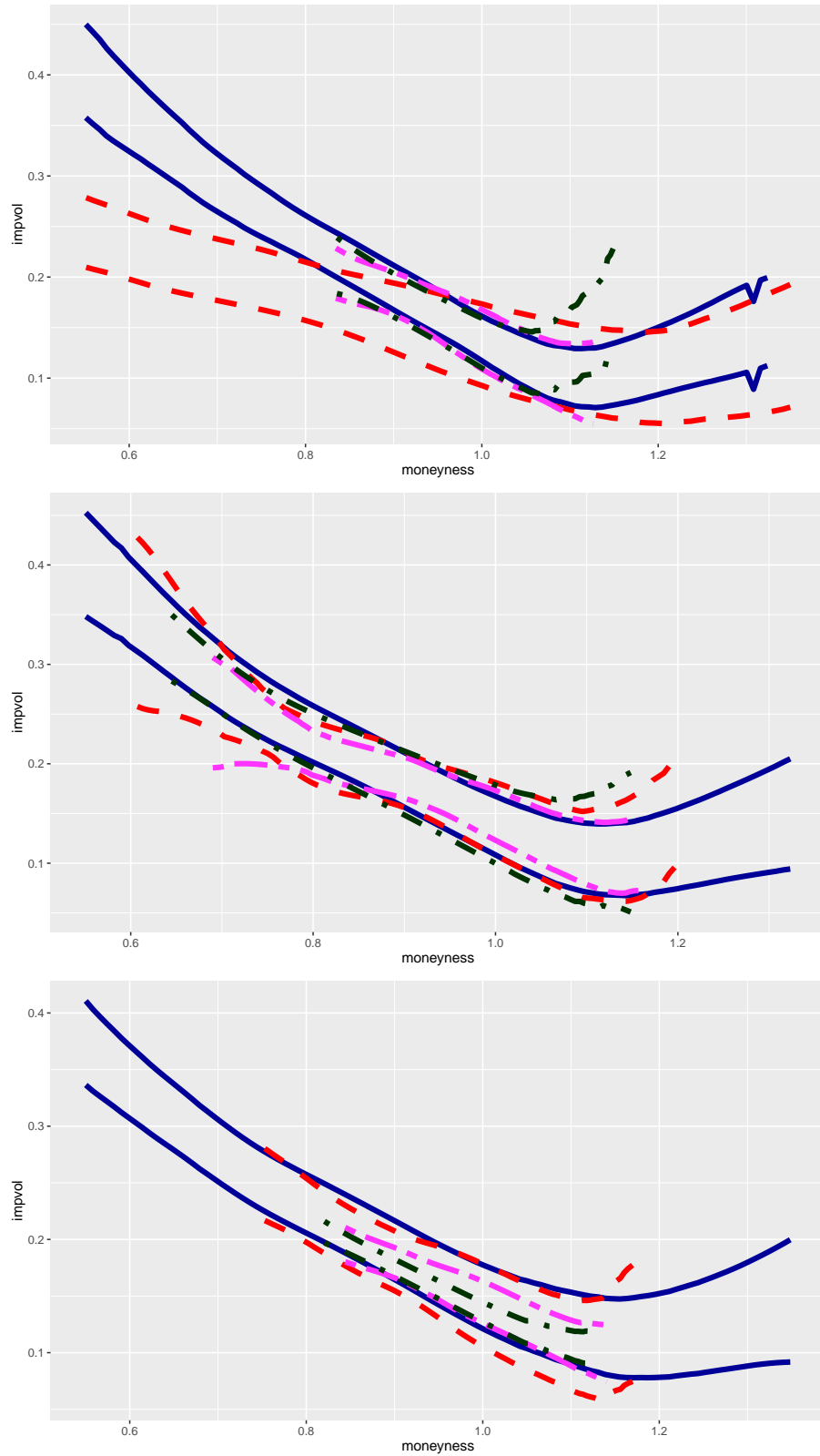
Figure 6: Combined uniform bootstrap confidence bands for SPY, SSO, UPRO and SDS after moneyness scaling
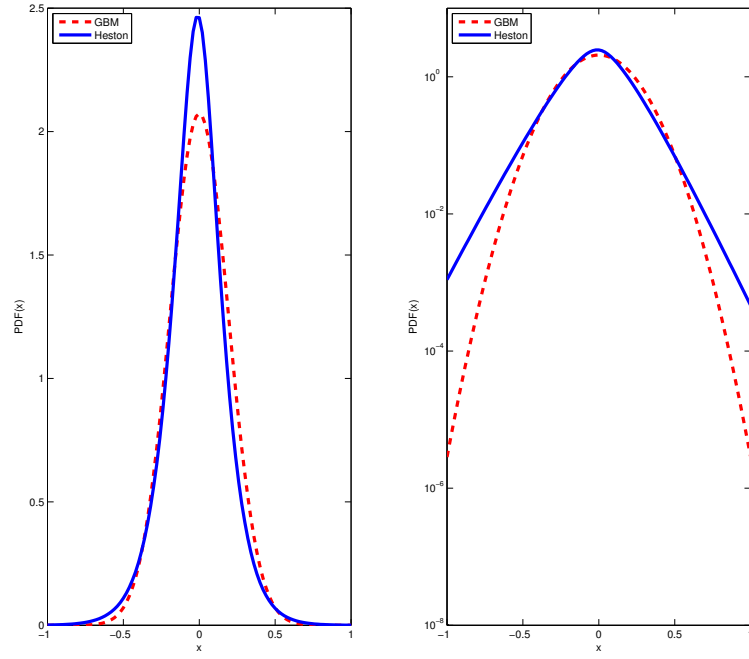
Figure 7: PDFs of log-returns implied by Heston and GBM, 20160201
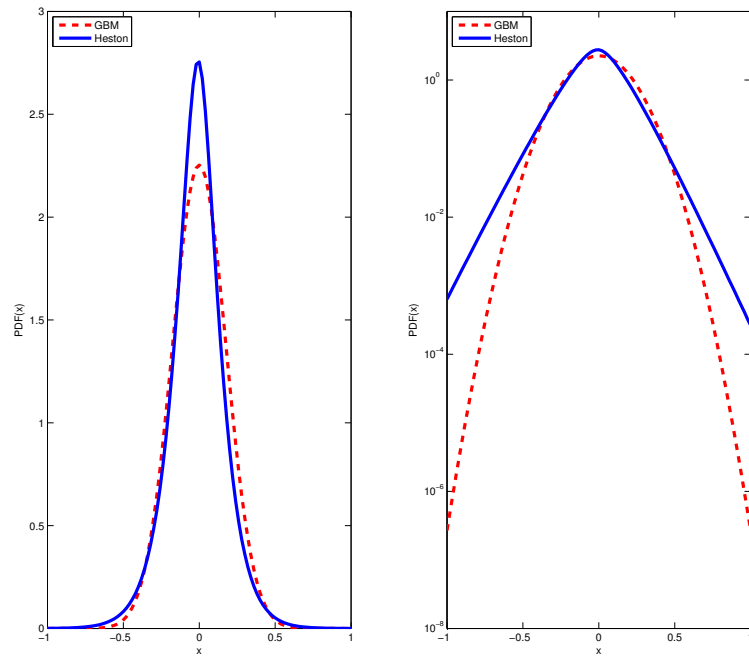
Figure 8: PDFs of log-returns implied by Heston and GBM, 20160205
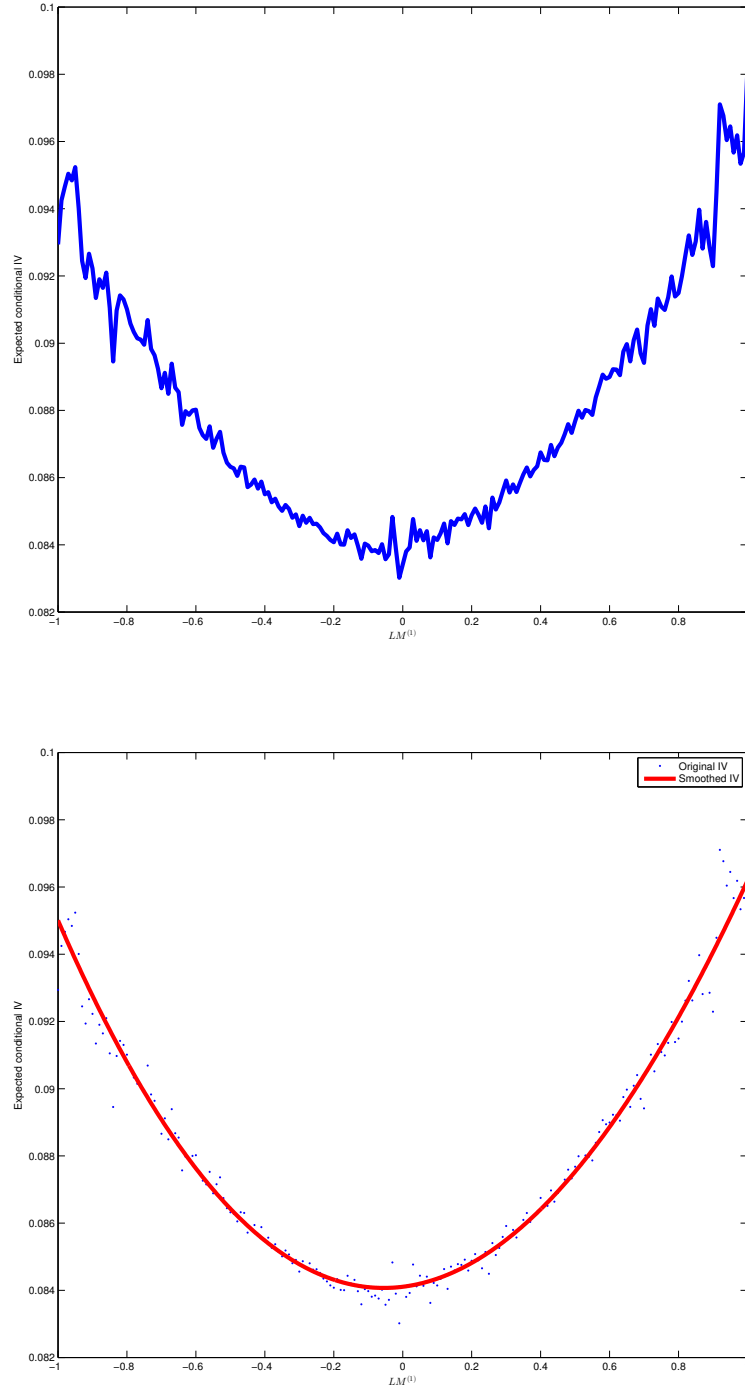
Figure 9: Upper panel: estimated value of $\mathbb{E}^{\mathsf{Q}}(\int_0^t \sigma_s^2 \mathrm{d}s|\log(L_t/L_0) = LM^{(1)})$; lower panel: smoothed estimate
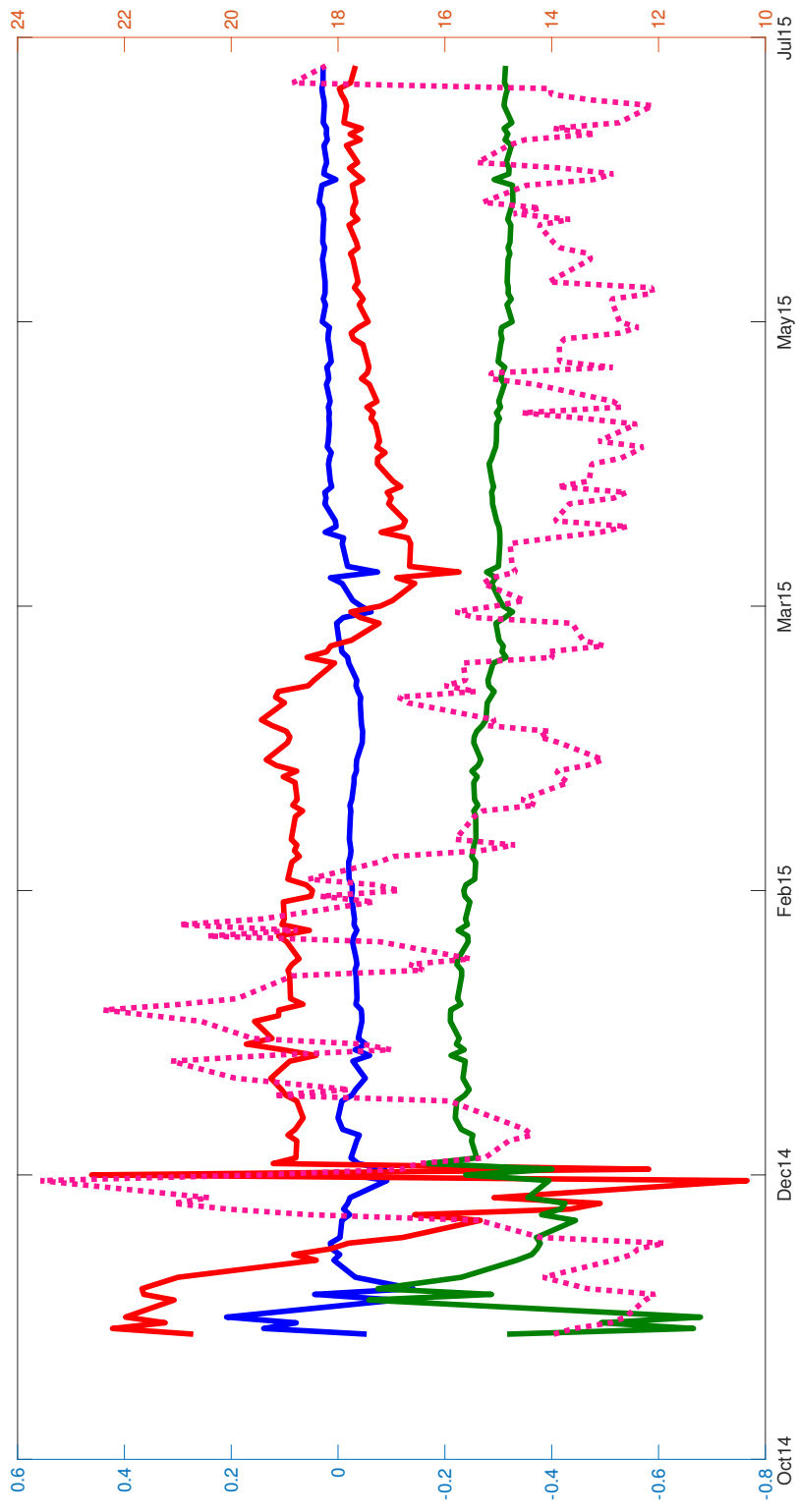
Figure 10: Time dynamics of $\widehat{\mathcal{Z}}_{t,1}$, $\widehat{\mathcal{Z}}_{t,2}$, $\widehat{\mathcal{Z}}_{t,3}$, VIX index
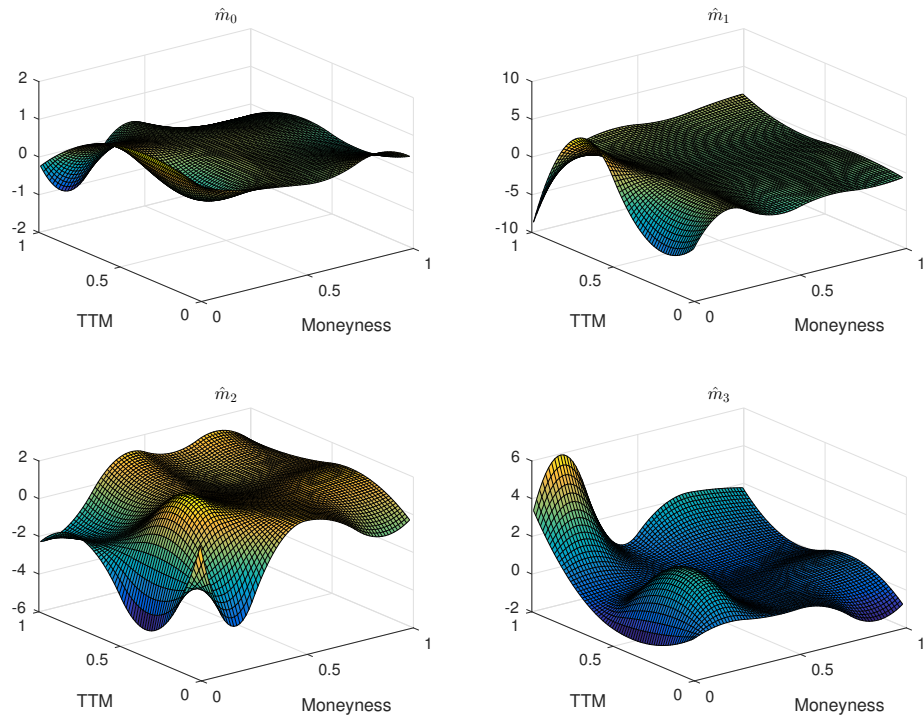
Figure 11: Factor functions $\hat{m}_0$, $\hat{m}_1$, $\hat{m}_2$, $\hat{m}_3$ for SPY option
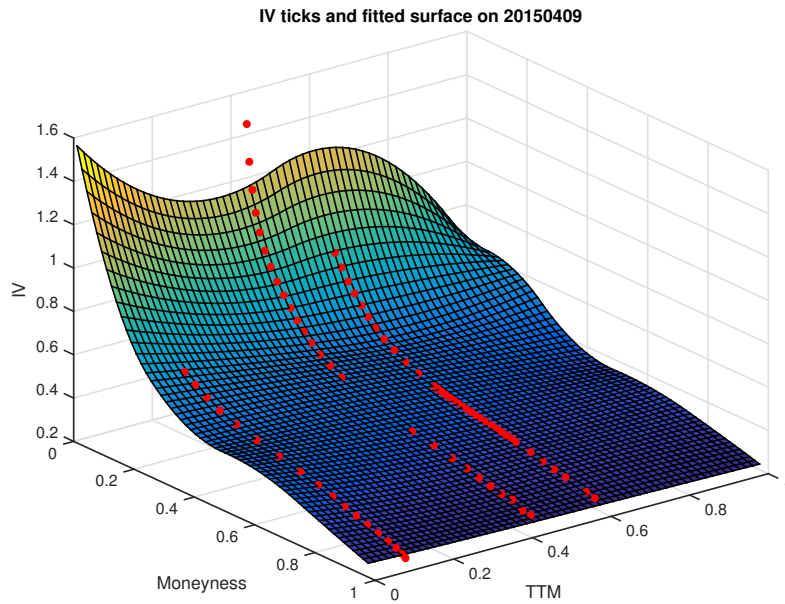
LETFFactorFuncs

Figure 12: Implied volatility real-data "strings" and the DSFM-fitted surface on 20150409
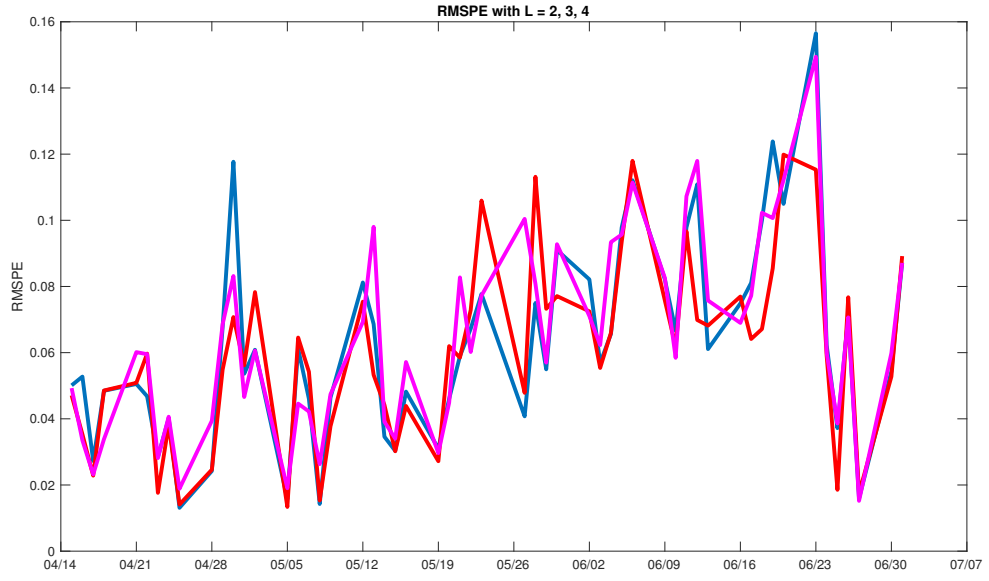
LETFIVSurfPlot

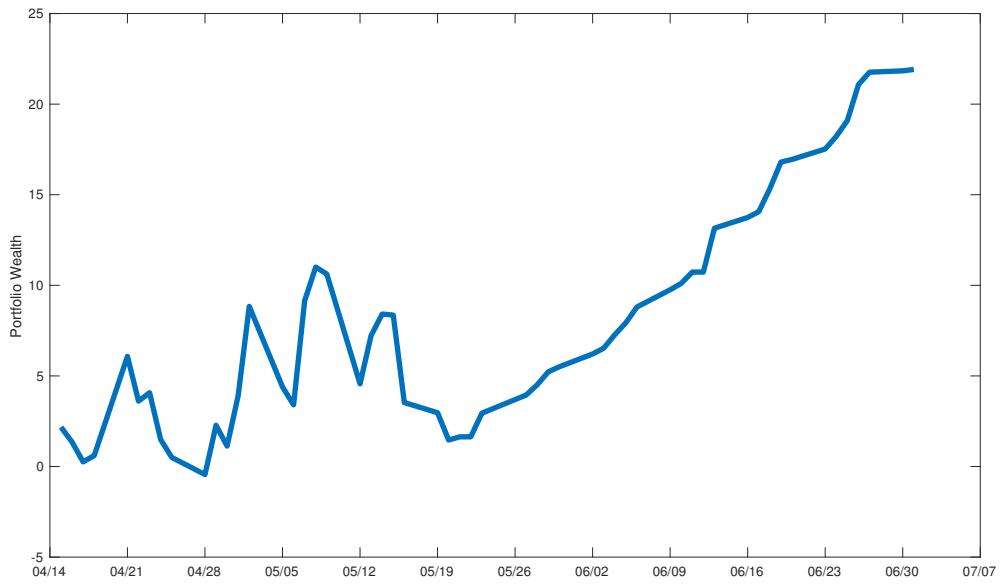Figure 13: RMSPE for $L = 2$, $L = 3$, $L = 4$ for the year 2015

Figure 14: Cumulative performance of the dynamic strategy for the year 2015

42